Modelling of a hybrid bioelectrocatalytic flow reactor with NADH cofactor regeneration by immobilized rhodium mediator for pyruvate bioconversion

Wassim El Housseini, Mathieu Etienne, Elisabeth Lojou, Alain Walcarius, François Lapicque

Modelling of a hybrid bioelectrocatalytic flow reactor with NADH cofactor regeneration by immobilized rhodium mediator for pyruvate bioconversion

Wassim El Housseini [1,3], Mathieu Etienne [1], Elisabeth Lojou [2], Alain Walcarius [1], François Lapicque [3 *]

[1] Université de Lorraine, CNRS, LCPME, 54000 Nancy, France

[2] Aix Marseille Univ, CNRS, BIP, UMR 7281, 31 Chemin Joseph Aiguier, CS 70071, 13402 Marseille Cedex 09, France

[3] Université de Lorraine, CNRS, LRGP, 54000 Nancy, France

Abstract:

The effectiveness of hybrid bioelectrocatalytic flow reactor with NADH cofactor regeneration by an immobilized rhodium mediator (*i.e.*, (2,2'-bipyridyl)(pentamethylcyclopentadienyl)-rhodium chloride complex, $[Cp^*Rh(bpy)Cl]^+$) was previously demonstrated for the example of pyruvate bioconversion with NAD^+ concentration as low as 10 µM. This paper presents a model of the complete hybrid process for NADH-based bioconversion, in view to identifying possible rate control by one of these phenomena depending on the operating conditions. For this purpose, the various phenomena involved in the 16 cm^2 bioelectrocatalytic cell, have been separately investigated, namely electrochemical reduction of immobilized Rh(III) complex, NADH regeneration by action of the formed Rh(I), mass transfer to the electrode layer and to the stacked enzyme loaded carbon layer, and lactate dehydrogenase-catalyzed pyruvate reduction by action of NADH. The kinetics of the redox process was shown to deviate from a first-order process with respect to NAD^+, resulting in a far larger reaction rate constant for the redox NADH regeneration with concentrations below 100 µM. Besides, simulations showed that in this concentration domain, far larger mass transfer coefficients to the carbon layers, had to be used to simulate the high production rate with the large turnover values observed: process intensification in the bioelectrochemical system allowed by the proximity of the two reactional layers, may explain far larger mass transfer coefficients.

Keywords: Flow reactors; bioelectrocatalytic processes; NADH regeneration; Rh complex; lactate dehydrogenase catalysis; Pyruvate bioconversion

Correspondence: Dr. Francois Lapicque francois.lapicque@univ-lorraine.fr

1- Introduction

NAD^+/NADH cofactor together with its phosphorylated derivative ($NADP^+$/NADPH) are electron mediators in a number of enzymatic catalyzed oxidation and reduction reactions [1, 2]. Because of its high cost, NADH has to be regenerated by suitable processes. Among them, electrochemical processes are very promising as they allow reaching high turnover numbers, without the use of sacrificial electron donors [3, 4]. Since NAD^+ cannot be directly reduced at an electrode surface in a biologically-active NADH form [5], its indirect reduction with a mediator such as coordination metal complexes, *e.g.*, Rh bi-pyridyl complexes [6], biological molecules or enzymes [4, 7], is carried out. For the case of (2,2'-bipyridyl)(pentamethylcyclopentadienyl)-rhodium chloride complex ($[Cp^*Rh(bpy)Cl]^+$), the electrolytic regeneration of NADH is often described by the two simplified reactions of a multistep process [8]:

$$Rh(III) + 2\ e \rightarrow Rh(I) \qquad (1)$$

$$Rh(I) + H^+ + NAD^+ \rightarrow Rh(III) + NADH \qquad (2)$$

where Rh(III) and Rh(I) designate the two mediator redox forms involved in the regeneration of NADH. Reaction (2) actually involves the intermediate formation of a hydride able to reduce NAD^+. More recent investigations related to hydrogen formation [9,10] or to specific dehydrogenations [11] showed by experiments and DFT calculations that the preferred site for the protonation of Cp*Rh(bpy) complex was not the metal center but the Cp* ligand. This ligand present in the complex appears not an innocent part, but actually plays a significant role in the overall NADH formation. In spite of the significant progress in understanding its mechanism, we preferred to consider reaction (2) as global in this work more dealing with chemical engineering: constant k_c mentioned in the paper is a phenomenological rate constant covering all occurring processes.

For the case of dissolved Rh complex, the kinetics of liquid phase reaction (2) was shown to be a fast chemical process, by interpretation of voltammetric curves of Rh(III) reduction in the presence of NAD^+ species. Assimilating the electrode surface to the gas-liquid interface [12], the model derived from multiphase reactor engineering with gas dissolution [13], led to estimates of the rate constant in the order of 30-50 $m^3\ mol^{-1}\ s^{-1}$ and showed that the chemical reaction occurred mainly in the electrode diffusion layer.

For the case of pyruvate reduction by NADH upon lactate dehydrogenase (LDH) catalysis, yielding lactate and NAD^+ species,

$$\text{Pyruvate} + \text{NADH} + H^+ \rightarrow \text{lactate} + NAD^+ \qquad (3)$$

the above Rh complex was successfully used either present in the electrolytic solution or immobilized on a carbon support in a hybrid flow reactor [14,15]. In particular for immobilized Rh complex, high yields in current and matter were obtained by low amounts of NAD^+/NADH with concentrations as low as 10 µM for the bioconversion of 25 mM pyruvate solutions [15]. Corresponding total turnover numbers (TTN) could attain 2500, 18000 and 180,000 for the NADH cofactor, the Rh complex and LDH enzyme, respectively, with a faradaic efficiency of lactate formation up to 79%. In addition to the desire to reach high cofactor TTN, the above figures of merits could be obtained in a hybrid flow bioreactor provided with a 16 cm^2 membrane electrode assembly consisting of a hydrogen gas flow anode for generation of H^+

$$H_2 \rightarrow 2\,H^+ + 2\,e^- \qquad (4)$$

required in NADH regeneration, a Nafion membrane and a carbon paper (CP)-based cathode coated with multiwalled carbon nanotubes (MWCNT) and electrochemically grafted Rh complex. Moreover, the LDH enzymes were immobilized on a second MWCNT-CP stacked onto the Rh-functionalized MWCNT-CP, the whole forming an active loop for the continuous regeneration of the cofactor for efficient pyruvate bioconversion as shown in Figure 1.

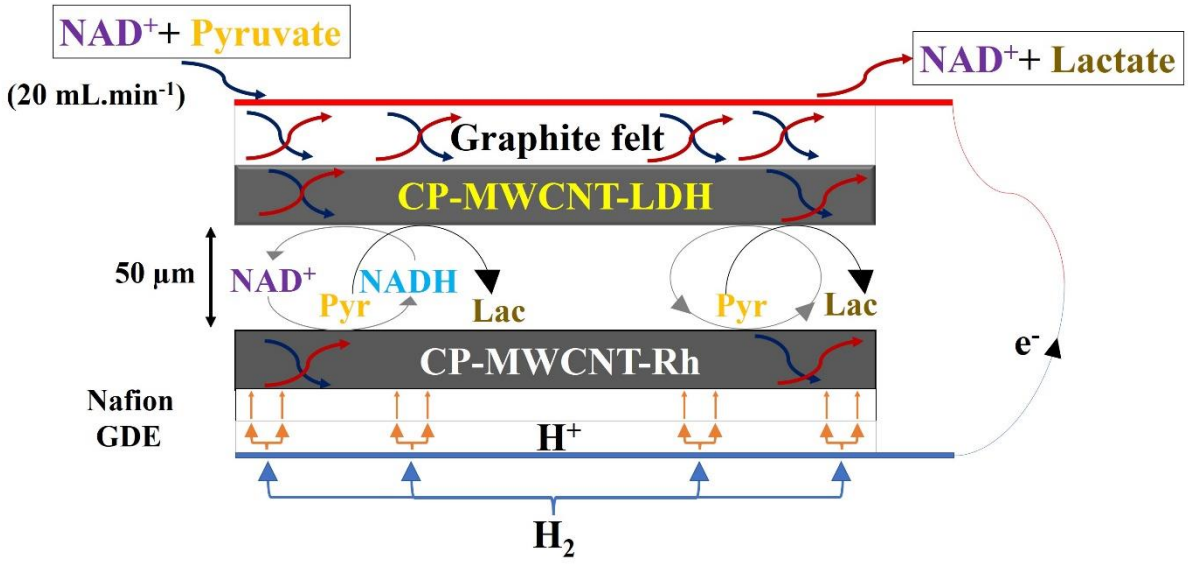

Figure 1: Schematic representation of the flow bioelectrochemical reactor. Lac and Pyr refer to lactate and pyruvate, respectively. GDE refers to Gas Diffusion Electrode.

LDH is a NAD-dependent dehydrogenase that reversibly converts lactate to pyruvate with the concomitant reduction of NAD^+ to NADH. In particular, for the case of pyruvate reduction by

NADH, the reaction rate upon LDH catalysis has been estimated to be 10^{14} times larger than without enzymes. Currently, LDH is still largely used for the production of chemicals, but more recent use is related to sensors [16-18] in association with redox couples or other enzymes. The great affinity of NADH and organic substrate molecules to LDH is due to the presence of a dedicated co-enzyme binding domain in the protein –sometimes referred as "Rossman fold" as in other dehydrogenases, together with a second site for binding the substrate. It is usually considered, that NADH is first bound to the enzyme structure through a multistep process, then the substrate (here pyruvate) can be bound onto the second side [19-22]. Binding of NADH to the substrate to be converted does not correspond to a simple diffusion from the bulk to the enzyme surface, but the approaching step of both types of molecules toward the enzyme is more a guided transport allowed by the protein bonding pocket using long-range electrostatic forces [19]. The overall binding of NADH onto LDH structure consists in several steps, with the formation of gradually better organised complex, with the existence of the so-called closed LDH-NADH complex by "diffusional encounter" [16], and an open LDH-NADH complex that could be suitable to pyruvate sorption [22]. After formation of LDH/NADH complex, the substrate is bound approx. 10 Å deep into the LDH/NADH complex on the substrate binding site [21]. This active site contains "crucial" His^{193} and Arg^{106} residues, and the preformed "pocket" can accommodate the pyruvate carboxylate group through the Arg^{169} side chain, as shown by Exequiel et al. [21].

The minimum distance between the various reactants and the enzymatic catalyst together with its immobilization on MWCNTs should be optimized to allow intensification of transfer and reaction phenomena. This concept largely mentioned in microscale chemical engineering [23] was also successfully applied by Scheller et al. [24], and by Limoges et al. [16, 25]. The two groups observed greatly amplified response of electrochemical biosensors to the presence of NADH or other analytes, owing to the proximity of diaphorase [25] and other immobilized enzymes or proteins, on the glassy carbon electrode using a dedicated immobilization procedure. Process intensification was also shown to be effective in a commercial flow bioreactor for H_2-driven biocatalysis using locally produced H_2 by water electrolysis [26].

The present work aimed at investigating the behaviour of the overall process with a hybrid bioelectrocatalytic flow reactor for NADH-based reduction of pyruvate with Rh complex mediation, to identify its rate-controlling part or step, in view to finding paths for improvement of the concept, then making it possible its application to other NADH-dependent bioconversions. The overall reduction of pyruvate in the 16 cm^2 electrochemical flow cell

consists of several steps, namely (i) electrochemical reduction of Rh(III) complex to Rh(I) species, (ii) chemical (redox) reaction between NAD^+ and Rh(I) to form NADH and Rh(III), (iii) enzymatic reduction of pyruvate to lactate, releasing NAD^+ in the solution, in addition to the various mass transfer processes to or from the electrode and the enzyme surface. For this purpose, each step of the process was studied, before a simulation tool could be developed for quantitative characterization of the whole process, through adjustment of parameter values through fitting experimental data to the model predictions. More precisely, we exploited data from cyclic voltammetry of Rh(I) formation, enzyme-free NADH production in the cell, electroless enzymatic pyruvate reduction by NADH, then finally long-term pyruvate reduction test with low NADH amounts. The methodology used, initially conventional since relying upon superimposition of the various phenomena of the process, had to be revised, to better take into account the intensification of transfer phenomena between the stacked CP-Rh electrode and the immobilized enzyme layer, together with the modified kinetics of the redox reaction between Rh(I) and NAD^+ for micromolar concentrations.

2- Experimental section

2.1. Chemicals used and analytical procedures

β-nicotinamide adenine dinucleotide (NAD^+, >98%) and β-nicotinamide adenine dinucleotide reduced dipotassium salt (NADH, >97%), $(RhCp^*Cl_2)_2$ (97 %), dichloromethane (DCM, 98 %), sodium nitrite (97 %), 2,2-bipyridine (98 %), 4-azidoaniline hydrochloride (98 %), K_2HPO_4 (99%), KH_2PO_4 (99%), HCl (37 %), L-lactate dehydrogenase (LDH) from bovine heart (≥ 250 units/mg protein, 144,000 Da.), pyruvate (98 %) and lactate (98 %), were from Sigma-Aldrich. Phosphate buffer solution (PBS, 50 mM, pH 7.2) was used to investigate the electrocatalytic properties of the Rh complex towards NAD^+ reduction and was reported to be the most appropriate for such experiments. Multiwall carbon nanotubes (MWCNT, NC7000™ series) were from Nanocyl (Belgium) and carbon papers (CP, SpectraCarb 2050L-0550 Carbon Paper) were acquired from Fuel Cell Store (USA). MWCNT were dispersed in a solution of ethanol (96 %). All solutions were prepared with high purity water (18 MΩ cm) from a Purelab Option water purification system. NADH was assayed by UV absorption at 340 nm. Pyruvate and lactate were analysed by HPLC, as described previously [14].

2.2. Hybrid bioelectrochemical reactor and its operation

The electrochemical reactor, with 4 x 4 cm^2 electrodes was previously developed [12, 14]. The reactor was fed continuously by a small hydrogen stream (20 Ncm^3/min) into the anode compartment, and the electrolytic solution was continuously recirculating in the cathode chamber at 20 cm^3/min. Protons generated at the hydrogen anode migrated towards the cathode through the 212 Nafion membrane. The cathode was a 127 µm thick CP coated with MWNCT (NC7000, Nanocyl) at 0.625 mg/cm^2 and supported by a macroporous graphite felt allowing the solution to be distributed over the cathode area. Rh complex was immobilized on the CNT surface following a formerly developed protocol [27], and reminded in the Supplementary Material. The resulting functionalized cathode was ascribed as CP-MWCNT-Rh.

The above cell was used for all tests considered in this work. For electroless enzymatic tests, the CP-MWCNT-Rh cathode was removed, whereas the enzyme coated CP MWCNT was not present for electrochemical tests being either cyclic voltammetry or NADH batch formation upon Rh mediation. No reference electrodes were mounted in the cell, but because of the very small change in the hydrogen anode potential, the anode could act as a reference electrode: cathode potential was thus referred to the anode and is expressed in this work in V vs. Ref. H_2. Voltammetric curves were recorded at 1 and 5 mV/s: from the third cycle, the electrode reaches fairly steady conditions, thus cycle 4 was usually retained for further interpretation.

3- Presentation of the models

Two main types of models have been developed here. The first sub-section presents models for interpretation of the voltammetric curves with emphasis of the current peak related to Rh reduction, and for discontinuous (batch) runs for NADH production by mediated reduction of NAD^+ species by the electrochemically reduced Rh complex. We present in the second sub-section models involving LDH catalysis, either for electroless pyruvate reduction by an introduced amount of NADH, or the lactate production in long-term runs by combined mediated electrochemical regeneration of NADH and its LDH-catalyzed action on pyruvate.

3.1. Electrochemical (enzyme-free) process

The Rhodium complex mediator is covalently attached to the high surface area porous carbon electrode. The fraction of grafted Rh in trivalent form, Rh(III), is called θ, the complement to unity (1-θ) being for electrogenerated Rh(I) species. The mole amount of Rh(III) is then equal to the product (ΓSθ) where Γ is the surface coverage with active Rh complex and S is the geometrical electrode area at 16 cm^2. In the following, A and B refer to NADH and NAD^+

species respectively. At the electrode surface, Rh(III) is electrochemically reduced to Rh(I) while NAD^+ is reduced by generated Rh(I): the surface chemical reaction was assumed to be a first-order process with respect to both Rh(I) and B species, with rate constant k_c (in $m^3\ mol^{-1}\ s^{-1}$). The transient mass balance in Rh(III) is thus written in the form:

$$\Gamma S \frac{d\theta}{dt} = -k_e \Gamma S \theta + \Gamma S k_c C_{B0}(1-\theta) \quad (5)$$

where k_e is the electrochemical rate constant in s^{-1} and C_{B0} refers to NAD^+ concentration at the electrode surface. The flux of NAD^+ reduced corresponds to that transferred from the bulk (subscript b):

$$k_L(C_{Bb} - C_{B0}) = \Gamma k_c C_{B0}(1-\theta) \quad ; k_L \text{ is the mass transfer coefficient} \quad (6)$$

from which surface concentration C_{B0} can be expressed as a function of NAD^+ concentration in the bulk:

$$C_{B0} = \frac{k_L C_{Bb}}{\Gamma k_c(1-\theta)+k_L} \quad (7)$$

Two types of experiments have been considered in the modelling.

Voltammetric curves

Bulk concentration C_{Bb} corresponds to the NAD^+ introduced in the solution prior to tests: C_{Bb} was assumed constant here. The cathode voltage was varied with rate v ($V\ s^{-1}$), from the equilibrium potential E_0 at t = 0. The electrode kinetics was assumed to obey a Butler Volmer expression involving parameter k_0 (in s^{-1}) and charge transfer coefficient α:

$$k_e = k_0 sinh\left[-\alpha n \frac{F}{RT}(E - E_0)\right] \quad (8)$$

Mass balance (2) was then rewritten under the form:

$$\frac{d\theta}{dt} = -2k_0 \sinh\left[\alpha n \frac{F}{RT} vt\right]\theta + k_c C_{B0}(1-\theta) \quad (9)$$

At initial time, grafted Rh is entirely in the trivalent form, so θ = 1. Equation (9) was numerically integrated taking into account rel. (7). Cell current I in the reduction (counted positive) at time *t* was calculated after:

$$I = I_{res} + 2F * 2k_0 \sinh\left[\alpha n \frac{F}{RT} vt\right]\Gamma S\theta \quad (10)$$

where I_{res} is the residual current, measured by voltammetry before grafting of the Rh complex on the CP-MWCNT support. Voltammetric tests conducted without added NAD^+ were used for

estimation of parameters k_0 and α, whereas other tests carried out in the presence of NAD^+ were used to estimate parameters k_c and k_L.

Batch regeneration of NADH

Potential E was kept constant from t = 0. Electrode rate constant k_e was calculated using rel. (7). Assuming that the residence time of the solution in the flow rig is far lower than the duration of the batch operation, the consumption rate of Rh(III) is simply expressed by:

$$V\frac{dC_{Bb}}{dt} = -k_c\Gamma S C_{B0}(1-\theta) \qquad (11)$$

where V is the volume of solution treated in the batch operation. Equations (5) and (11) were integrated taking into account rel. (7): at initial time, surface Rh equilibrium was assumed, so θ(t=0) was calculated from rel. (5) neglecting the transient left term and using rel. (7). Current was calculated at time t using rel. (12).

$$I = I_{res} + 2Fk_e\Gamma S\theta \qquad (12)$$

3.2. Enzymatic reaction involving models

Enzymatic reaction kinetics was first investigated through electroless tests for consumption of given amounts of NADH and pyruvate upon LDH catalysis. The reaction model proposed here was inspired from previous works with Michaelis-Menten-like models, relying in particular on the sequence of binding steps [19-22]: NADH was assumed to be first bound to the LDH structure, then pyruvate substrate was bound deeply into the LDH/NADH complex. Here below E and P designate respectively the enzyme and pyruvate. The model proposed thus involved the successive formation of the two intermediate complexes EA and EAP, and assuming that formed EBQ decomposed instantaneously to E, B and Q (here lactate), as schemed in Figure 2.

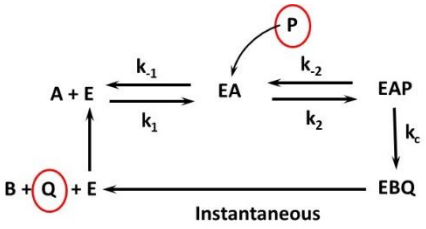

Figure 2: Two-step formation of complex EAP, i.e., after formation of first complex EA for formation of Q and back-releasing of NAD+ (B) and LDH enzyme E

The concentrations of intermediates EA and EAP were assumed constant in the discontinuous tests, yielding the two equations below:

$$V\frac{dC_{EAs}}{dt} = k_1 C_{As} C_{Es} - k_{-1} C_{EAs} - k_2 C_{EAs} C_{Ps} + k_{-2} C_{EAPs} = 0 \qquad (13)$$

$$V\frac{dC_{EAPs}}{dt} = k_2 C_{EAs} C_{Ps} - k_{-2} C_{EAPs} - k_c C_{EAPs} = 0 \qquad (14)$$

where subscript corresponds to the surface of the enzyme support. Because LDH is immobilized on a support, surface concentration (in mol m^{-2}) should be used. However, concentrations of all LDH-related species are here volume concentrations in mol m^{-3}, related the molar amounts of this species and the solution volume V. Mass balance on enzyme-containing species is also written:

$$C_{E0} = C_{Es} + C_{EAs} + C_{EAPs} \qquad (15)$$

where C_{E0} is the enzyme (volume) concentration, related to the amount of immobilized enzyme. Finally, the rate of pyruvate conversion is expressed as:

$$V\frac{dC_{Pb}}{dt} = -Vk_c C_{EAPs} \qquad (16)$$

Concentrations at the electrode surface for species A and P can be related to their respectively bulk concentrations using mass transfer coefficient k_d, which was considered to be at the same value for the two species:

$$V\frac{dC_{Pb}}{dt} = k_d(C_{Pb} - C_{Ps}) = k_d(C_{Ab} - C_{As}) \qquad (17)$$

Finally, the maximum reaction rate v_{max} per area unit is defined by:

$$Vk_c C_{E0} = Sv_{max} \qquad (18)$$

Combining rel. (13)-(17) and taking into account rel. (18) led to:

$$V\frac{dC_{Pb}}{dt} = -S\frac{v_{max}}{1+\frac{K_{M2}}{C_{Ps}}\left(1+\frac{k_{-1}+k_2}{k_1 C_{As}}\right)-\frac{k_{-2}}{k_1 C_{As}}} = -S\frac{v_{max}}{1+\frac{K_{M2}}{C_{Ps}}\left(1+\frac{K_{M1}}{C_{As}}\right)-\frac{K_2 K_{21}}{C_{As}}} \qquad (19)$$

where constants K_1, K_2, K_{21} and K_{M2} are defined as follows:

$$K_2 = \frac{k_{-2}}{k_2} \qquad K_{21} = \frac{k_2}{k_1} \quad K_{M1} = \frac{k_{-1}+k_2}{k_1} = K_1 + K_{21} \qquad K_{M2} = \frac{k_{-2}+k_c}{k_2} \qquad (20)$$

Constants K_1 and K_2 are the dissociation constants of complexes EA and EAP respectively, K_{21} is the ratio of the rate constants of complex formation (EAP and EA), and K_{M1} and K_{M2} are Michaelis-Menten constant related to complex EA and EAP. The model for electroless

enzymatic pyruvate reduction involves the following parameters: k_d, v_{max} , K_1, K_2, K_{21} and K_{M2} (since K_{M1} is the sum of K_1 and K_{21}).

In long-term runs for lactate production, rel. (19) is also used to express the consumption rate of pyruvate. In addition, time variation of NAD^+ concentration is caused by its formation in the enzymatic process and its consumption through chemical reaction at the electrode surface:

$$\frac{dC_{Bb}}{dt} = -\frac{k\Gamma S}{V} C_{Bs}(1-\theta) - \frac{dC_{Pb}}{dt} \qquad (21)$$

Variations of the solution composition and of the cell current were calculated by solving eq. (19), (21) and (12).

4- Results

4.1. Electrochemical (enzyme-free) processes

Three series of experiments have been carried out, each with freshly prepared Rh-deposited cathodes (C1-C3). The Rh surface concentration estimated by cyclic voltammetry, Γ, was found at nearly 10 nmol cm^{-2} for C1 and C2, and 5 nmol cm^{-2} for C3. The voltammetric curves with deposited Rh were corrected by subtracting the residual current recorded on the MWCNT-CP electrode. This current depicted in Figure 3a is presumably the fact of reduction processes of oxygenated functions on the carbon support, and to hydrogen side-evolution for potentials more cathodic than -0.4 V. Equilibrium potential was usually in the range -0.05 / -0.10 V vs. Ref. H_2 (Figure 3a). The current peak observed near -0.35 V vs. Ref. H_2, corresponds to the reduction of Rh(III). Raw and corrected curves differed in a significant manner as exemplified in Figure 3a. Moreover, the presence of NAD^+ resulted in larger currents (Figure 3a and 3b) because of the chemical redox reaction consuming the electrogenerated Rh(I) species, as reported previously [14].

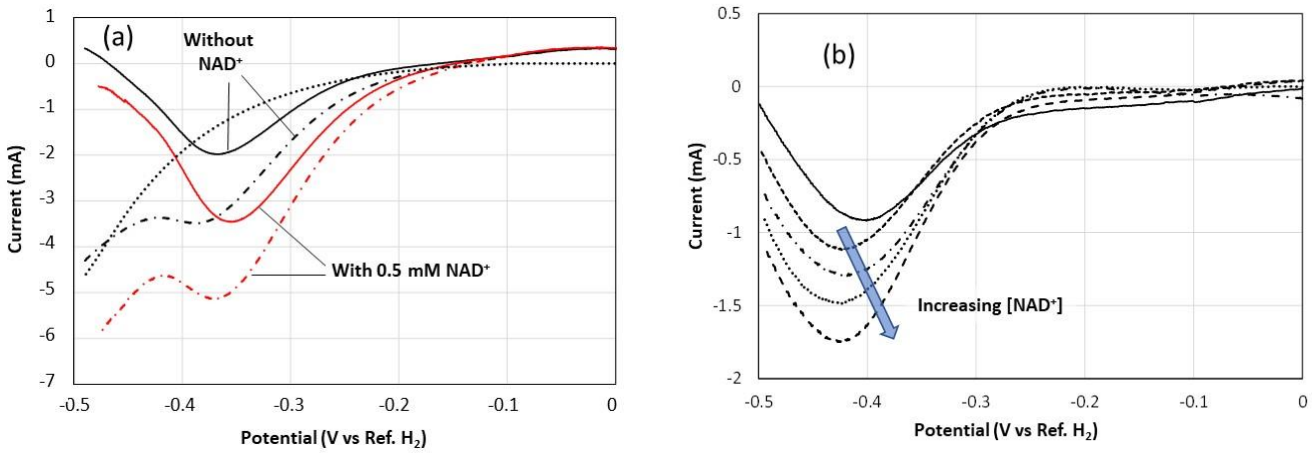

Figure 3: Examples of voltammetric curves:

a) left, voltammograms recorded on C2 at 5 mV/s, Γ = 4.152 nmol cm^{-2}, with (red curves) or without NAD^+ (black curves). (**.....**): residual current; (_ _ _): raw voltammograms, (_____): corrected curves.

b) right, corrected voltammograms recorded on C3 at 5 mV/s, Γ = 2.62 nmol cm^{-2}, effect of NAD^+ concentration. (_____): no NAD^+; (**.....**): 0.5 mM; (_ _ _): 1 mM; (.....): 2 mM; (- - - - - -): 3 mM

Interpretation of the CV curves without NAD^+ led to α value at 0.30 within 0.02, with rate constant k_0 between 0.2 – 1. 10^{-4} s^{-1}, for the three cathodes tested. Figure 4 gives an example of experimental and fitted voltammetric curves.

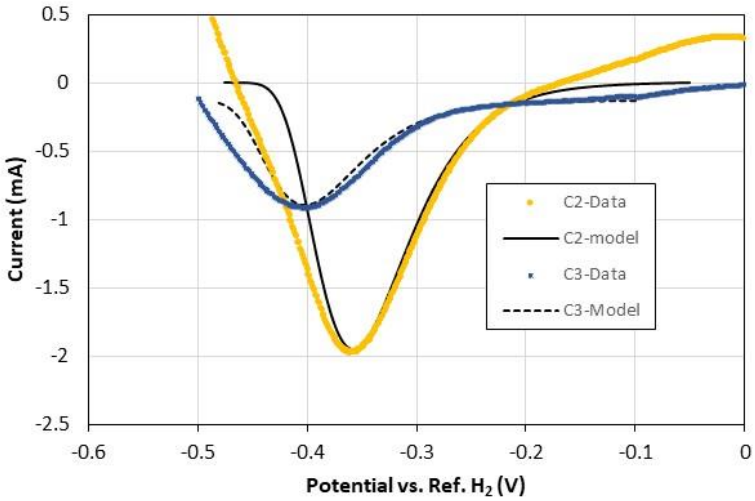

Figure 4: Predicted and experimental voltammograms recorded at 5 mV/s of two Rh-grafted cathodes, with Γ values at 4.152 nmol cm^{-2} for C2, and 2.62 nmol cm^{-2} for C3.

In the presence of NAD^+, fitting of the various sources of data yielded estimates for k_c ranging from 0.05 to 0.15 $m^3\ mol^{-1}\ s^{-1}$, with mass transfer coefficient k_L between 0.5 and 1 10^{-4} m s^{-1}. The peak profile was affected by the two parameters; whereas the effect of k_c on the peak current is large – with a nearly linear variation between k_c and I(peak), increasing the transfer coefficient k_L by 50% results only in a 20% increase in the current. It can be observed that the redox rate constant estimated here is orders of magnitude below the values found with dissolved Rh [9]. This strong difference is likely due to the different states of Rh in the two investigations, with possible different/lower reactivity of deposited Rh than dissolved metal complex [28], and to more troublesome access of NAD^+ species to formed Rh(I) complex on the porous MWCNT-CP cathode. Values for k_L in the order of 10^{-4} m/s do not express any turbulent flow but are mainly due to the fact that the cathode active area is far larger than the geometrical area S used here for calculations.

Batch NADH regeneration experiments have been conducted with the three cathodes: for cathode C1, the NAD^+ concentration was at 1 mM, with a solution volume at 20 cm^3, and for the two other cathodes, NAD^+ was introduced at 0.5 mM and the volume was 40 cm^3. The potential was fixed at -0.3 or -0.35 V vs Ref. H_2, the current and the charge were monitored, and UV-analysis of the samples taken led to NAD^+ concentrations. The current efficiency was calculated from the mole amount of NADH formed and the charge passed. The introduced NAD^+ amount could be fully reduced to NADH within one hour or so (Figure 5). As expected, the conversion with cathode C3 was slower because of the two-time lower amounts of Rh deposited. The current monitored was in the range 1.5 -3 mA in absolute value.

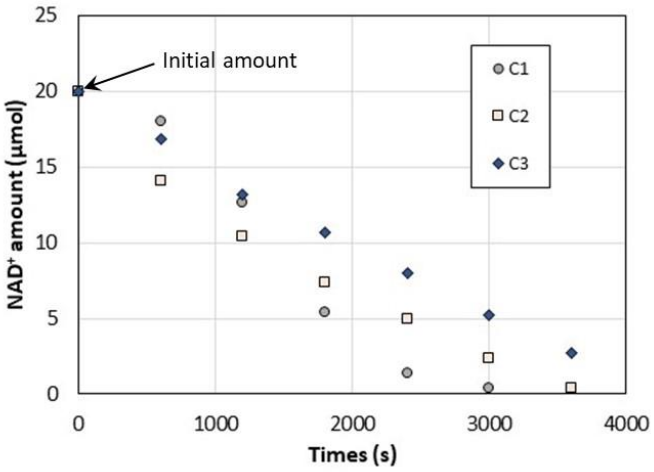

Figure 5. Experimental variations of NAD^+ mole amounts in batch electrochemical reduction runs with deposited Rh complexes at fixed potential (-0.35 V vs. Ref. H_2).

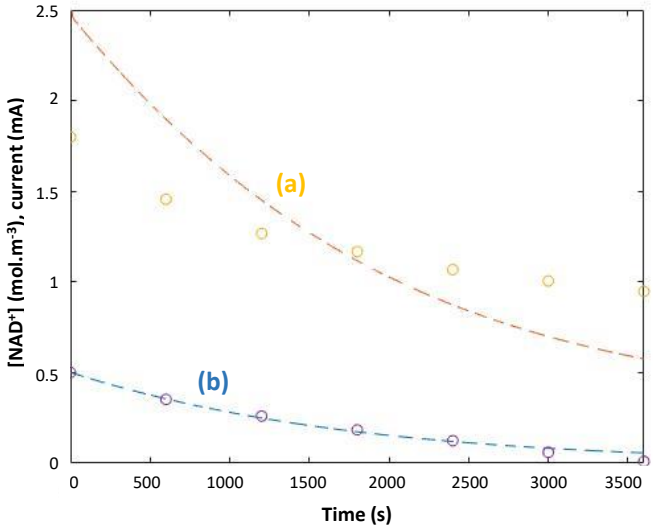

Figure 6: Experimental and predicted variations of the current in absolute value (a) and NAD^+ concentration (b) in the tests carried out with cathode C2 at fixed potential (-0.35 V vs. Ref. H_2).

For each run, current values experimentally obtained and NAD^+ concentration were fitted by the model, by letting varied k_e, k_L and k_c. For the three tests, satisfactory fitting was obtained as shown in Figure 6 for the case of C2 cathode with $k_L = 10^{-4}$ m s^{-1}, $k_e = 0.5$ s^{-1} and $k_c = 0.2$ m^3 mol^{-1} s^{-1}. Rate constant k_c exerts a strong effect on the model predictions, so does k_e to a lower extent, whereas k_L affects more the current value than the concentration profile. The confidence intervals for the three parameters were estimated at 20% for k_c, 30 for k_e and approx. 40 % for k_L. The value for k_e is somewhat larger than the value deduced from rel. (7) with the above given values for α and k_0, equal to 0.12 and 0.40 depending on whether E was fixed at -0.3 or -0.35 V vs. Ref. H_2. This value is nevertheless consistent with that estimated in a former work [27].

4.2. LDH-assisted electroreduction of pyruvate

Electroless enzymatic tests

The electrochemical model developed above and applied here to lactate hydrogenase, has been tested under various conditions, in particular in a large range of pyruvate concentrations. For pyruvate concentrations near 1 mM or above, we observed slightly slower oxidation of NADH related to pyruvate reduction by lactate dehydrogenase (LDH), indicating a possible inhibition by pyruvate. As a matter of fact, inhibition of enzymatic processes by chemical substances is

often reported, in particular for LDH. Because pyruvate concentrations over 12.5 mM had been considered in the overall process with NADH regeneration [12], it was decided to add an inhibition term, with constant k_i in mol m^{-3} into the original model presented before.

The three typical batch experiments retained for estimation of the various model parameters, were carried out with 40 mL PBS solution at pH 7.2 containing 0.2 mM NADH in contact with pyruvate at 0.2, 1 and 10 mM, in the presence of 250 LDH units (approx. 0.995 mg) immobilized on a MWCNT-CP support with an area at 9 cm^2. All tests were carried out at ambient temperature. It was preferred to operate here with appreciable NADH concentrations, larger than those long-term runs, for the sake of sufficient accuracy in NADH analysis by UV absorption at 340 nm. Figure 7 shows the experimental data together with the predicted variation, with the following parameter values:

v_{max} = 3.3 10^{-5} mol m^{-2} s^{-1} (S = 9 cm^2); k_d = 10^{-3} m s^{-1}; K_1 = 0.02 mol m^{-3}, K_2 = 0.002 mol m^{-3}, K_{21} = 0.02, K_{M2} = 0.03 mol m^{-3} and k_i = 6 mol m^{-3}

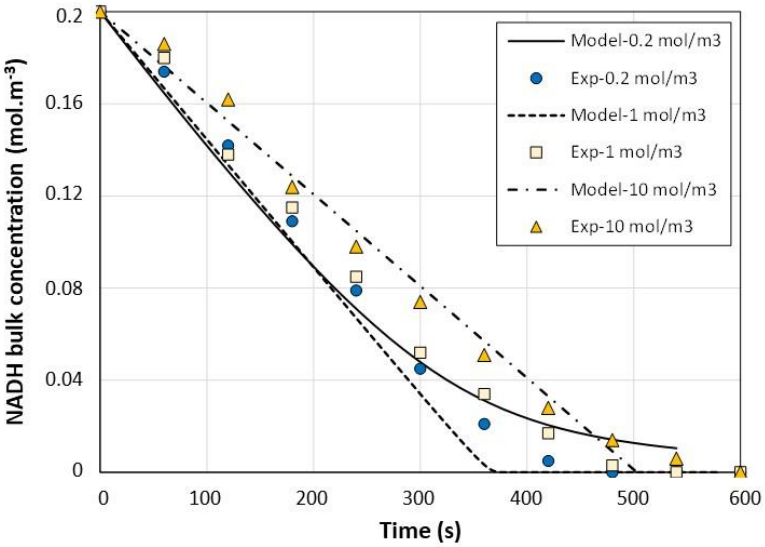

Figure 7: Kinetics of NADH oxidation by pyruvate upon LDH catalysis. V = 40 mL PBS solution pH=7.2 with pyruvate at various concentrations and NADH (0.2 mol. m^{-3}). LDH amount = 250 Units (0.995 mg on 9 cm^2 CP-MWCNT support)

The value for v_{max} corresponds here to approx. 0.03 µmol s^{-1} mg^{-1} LDH. Although somewhat lower than values reported in the literature [20, 29], the estimate for v_{max} on the CP-MWCNT support appear to be of an acceptable agreement, considering the particular 3-dimensional nanometric support.

Electro-enzymatic reduction of pyruvate mediated by NADH and immobilized Rh complex

The various modelling parts have been assembled in view to simulating long-term production of lactate by LDH-catalyzed reduction of pyruvate with continuous regeneration of NADH with mediation of immobilized Rh complex. Here, for the sake of large production with a high total turnover (TTN), it was preferred to considered low NADx amounts (covering NAD^+ and NADH species), down to 10 µM, while treating concentrations of pyruvate at 10 mol m^{-3} or more. Here, amongst the various conversion tests carried out in the lab, two experiments were analysed, one with 100 µM NADx and 12.5 mM (mol m^{-3}) pyruvate, the other with only 10 µM NADx with the same initial pyruvate concentration. In both tests, 100 cm^3 solution were gradually treated with a fixed potential of the cathode (-0.3 V vs Ref. H_2), only one 16 cm^2 electrode was used, and 250 LDH units were deposited onto the 16 cm^2 CP-MWCNT support. For the 3-day long runs considered here, TTNs with respect to Rh, NADH and LDH were found respectively at 10,000, 73 and 100,000 for the experiment with 100 µM NADx, whereas they respectively attained 9,200, 640 and 92,000 for the run with the lower NADx concentration. The time variations of pyruvate concentrations are reported in Figure 8. What could be observed is that even with very low amount of NAD^+, pyruvate reduction can be processed with a large rate.

The reduction rate decreased regularly over time (Figure 8). For the two first hours, the concentration of pyruvate decreased at 0.9 and 1.3 mM/hour with 10 and 100 µM NADx in the solution (Figure 8). The reduction rate appears to be far from a linear function of NADH concentration, presumably because of the likely intensification of combined reaction and transfer processes at the stacked electrodes and enzyme supporting layer.

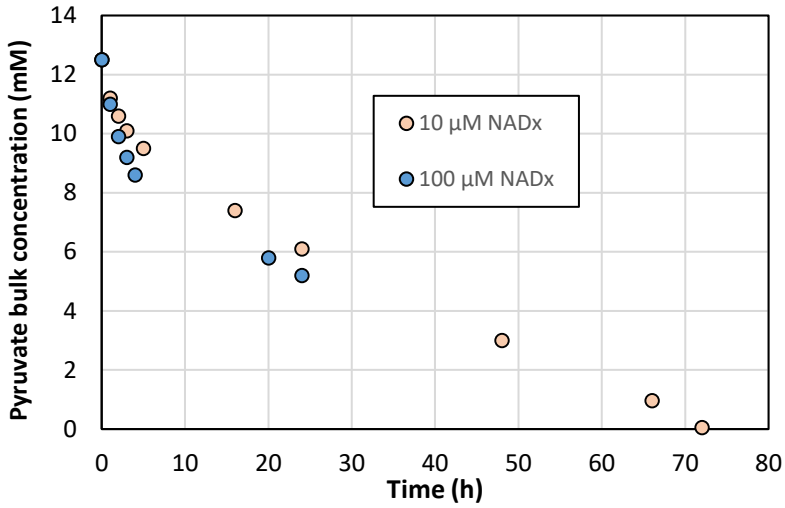

Figure 8: Examples of long-term runs of LDH-catalyzed pyruvate reduction. V = 100 mL, S = 16 cm^2, 250 LDH units, $E_{cathode}$ = -0.3 V vs. Ref. H_2.

We first used the parameters estimated in the various sections described above. Such attempts greatly underestimated the conversion rates. Because of the combined electrochemical, chemical, enzymatic reactions and transfer phenomena in a sub-millimetric scale or below, the high conversion rates in the first hours with low concentration of NADx species together with the high TTN, suggest the existence of strong process intensification in the bioelectrochemical cell, with far larger mass transfer coefficients. Such intensification was also demonstrated by Limoges et al. [25] for their combined electroenzymatic sensors with huge amplification of the electrical current. More recently, intensification of the production rate for H_2-driven pyruvate reduction was observed in a bioelectrochemical reactor whose cathode was stacked to the enzyme support and operated with flow recirculation [26] Very high TTN (up to 800,000 with respect to LDH) and turn over-frequency were there reported.

For the present case, the conversion rate has to be equal to the mass transfer rate of NAD^+ to the electrode surface and the rate of chemical reaction between Rh(I) complex and NAD^+ at the electrode surface as in rel. (6):

$$Conversion\ rate = k_L S(C_{Bb} - C_{B0}) = \Gamma S k_c C_{B0}(1-\theta) \qquad (22)$$

Because concentrations C_{Bb} and C_{B0} are lower than C_{NADx}, rel. (22) leads to the following inequalities:

$$k_L > \frac{Conversion\ rate}{SC_{NADx}} \qquad (23a)$$

$$k_c > \frac{Conversion\ rate}{\Gamma SC_{NADx}} \qquad (23b)$$

For the two long-term runs shown, the values for k_L and k_c estimated in the preliminary specific experiments, in the order of 10^{-4} m s^{-1} and 0.1 m^3 mol^{-1} s^{-1} respectively, are far too low to predict the experimental variations of pyruvate concentrations, with the low amounts of NADx employed. Moreover, considering values for k_c not fulfilling rel. (23b) in simulations is to lead to conversion rates of pyruvate noticeably below the experimental observations, making the interpretation of experiments impossible.

Mass transfer coefficient at the electrode

The superimposition of electrochemical and chemical processes at the electrode surface can explain the apparent far larger mass transfer coefficient. To avoid too significant control by mass transfer, it was preferred to postulate $k_L = 10^{-3}$ and $5\ 10^{-3}$ m s^{-1} for NADx concentration at 100 and 10 µM, respectively. Simulation tests with two times larger k_L values resulted in a few percent changes in the variations, except for fraction θ of Rh(III) complex where +11% change was observed. Besides it can be observed that transfer rate to the enzyme surface would have to fulfil comparable constraint. However, as explained above, transfer rate of NADH and pyruvate do involve the contribution of attraction forces between the enzyme active sites and the two molecules. Because this work was not aimed at determining accurate values for all parameters in a particular reactor configuration, but to identify the rate controlling steps in the pyruvate conversion, it was preferred in the simulations to neglect mass transfer control at the enzyme, so that surface concentrations C_{Xs} were approximated at their levels in the bulk, for X=NADH and pyruvate.

The intensification of the process observed above can be explained by the fact that LDH is stacked between two layers of MWCNT: LDH is immobilized on the first layer whereas the second one supports the Rh complex. The presence of two layers of MWCNT facilitating the grafting of the two catalysts, together the graphite felt electrode is to reduce the distance between the two active areas in the cathodic compartment. The hypothesis was confirmed for NADH regeneration: addition of a second CP-MWNCT without Rh complex, resulted in regeneration rate two times larger than those obtained with the single CP-MWCNT-Rh cathode, as reported in the Supplementary Material, Fig. S1.

Chemical rate constant of NADH formation

Simulations have been conducted for the first six hours of the runs since the models do not account for the deactivation of the enzyme, causing visible slowing down of the enzymatic conversion. The average conversion rate attained 1.25 and $1.75\ 10^{-8}$ mol s^{-1} using 10 and 100

µM NAD^+ solution. Trial and errors tests have been made for estimation of a few model parameters, namely v_{max}, k_e and k_c. For the two tests, v_{max} was estimated at 2 10^{-5} mol m^{-2} s^{-1}, i.e. 0.032 µmol s^{-1} mg^{-1} LDH and k_e at 0.5 s^{-1} in acceptable agreement with the electrochemical experiments reported in Section 4.1. The v_{max} value are also consistent with that Poznansky et al. 2021, with their large-scale test with 5 mg LDH. Rate constant k_c was estimated at 13 and 2 m^3 mol^{-1} s^{-1} for NADx concentration at 10 and 100 µM respectively. To check the validity of the above hypothesis, replicate enzyme-free NADH regeneration tests have been performed with NADx concentration at 100 µM, with a freshly immobilized Rh complex on a CP-MWCNT support. The experimental setup used did not allow tests with lower NADx concentration for sufficient accuracy. In spite of the low NADx concentration, the regeneration rate of NADH was larger than with 0.5 mM in the three runs (Supplementary Material, Fig. S2), leading to apparent rate constant k_c in the range 2 – 3.5 m^3 mol^{-1} s^{-1}.

Although the reduction kinetics of NAD^+ by Rh(I) has been considered in the model as a first-order process with respect to NAD^+, former works on the reaction kinetics suggested a Michaelis-Menten process [30] with a K_M constant for NAD^+ in the order of 9 mM [7]. Therefore, such a kinetics – although not fully admitted in the community-, would mean that the apparent reaction rate (with a reaction rate proportional to C_{B0}) could be quite larger for lower NAD_x concentration. Moreover, possible deactivation of grafted Rh species by NADx present at mM levels cannot be excluded.

Figure 9 presents the simulation results for the run with 10 µM NADx, in terms of pyruvate bulk concentration, cell current, coverage fraction θ related to trivalent Rh complex on the electrode and the relative significance of NAD^+ in the solution bulk. The experimental variations of the pyruvate concentration and cell current are also given.

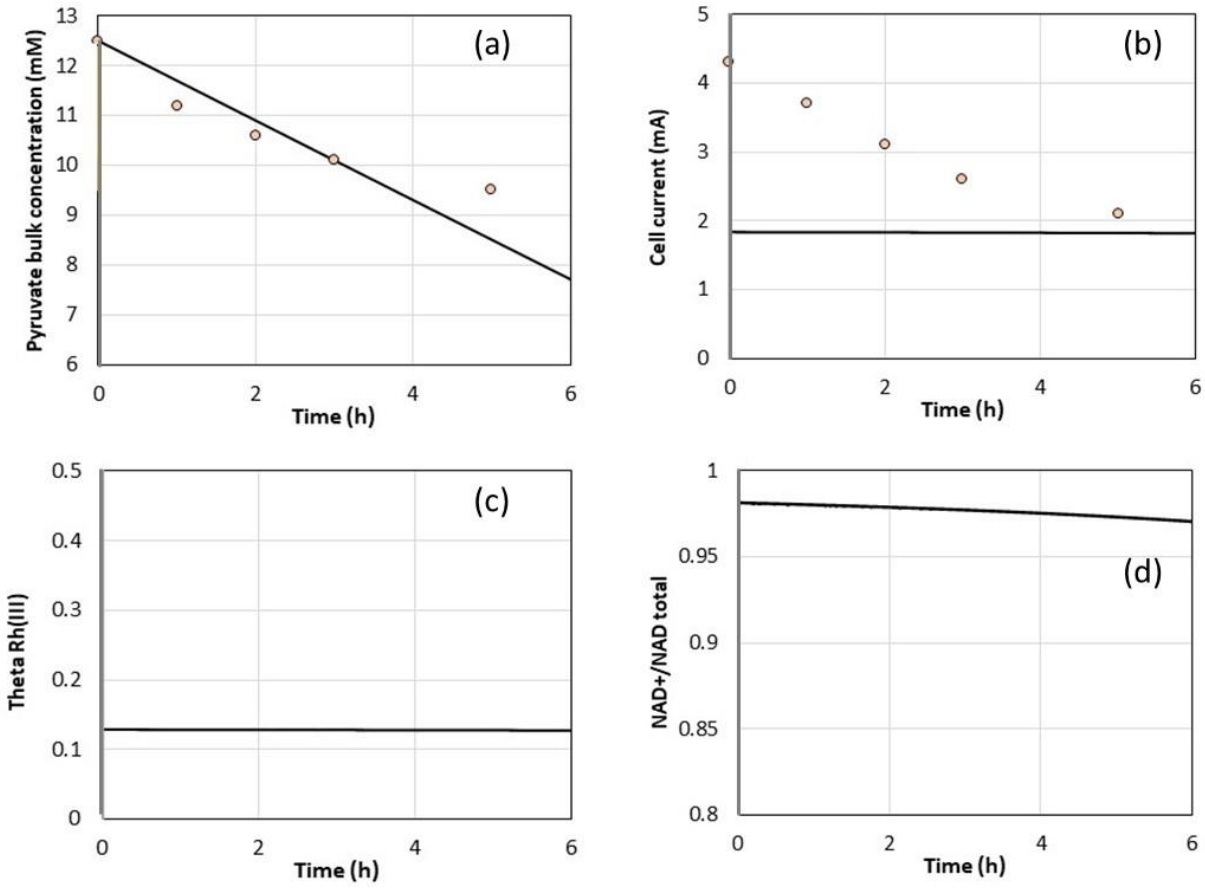

Figure 9: LDH-catalyzed reduction of pyruvate with Rh complex and NAD^+/NADH mediation in the flow reactor. (a) experimental and predicted pyruvate concentration; (b) experimental and theoretical cell current; c) Calculated Rh(III) fraction θ; (d) calculated relative importance of NAD^+ in the cofactor concentration. NADx concentration at 10 µM, Solution volume = 100 mL, area S = 16 cm^2, $E_{cathode}$ = -0.3 V vs Ref. H_2. Kinetic parameters values: v_{max} = 2 10^{-5} mol m^{-2} s^{-1}, i.e. 0.032 µmol s^{-1} mg^{-1} LDH, k_e = 0.5 s^{-1} and k_c =13 m^3 mol^{-1} s^{-1}.

Whereas simulation and practice led to decreasing pyruvate concentrations over time in the long-term test (Fig. 9a), and in spite of the decreasing profile of the current monitored (Fig. 9b), the model of the flow bioelectrochemical cell shows that most variables, *e.g.*, current, surface fraction θ and the significance of NAD^+ remained fairly constant in the day-long run (only 6 hour period shown here, Fig. 9b-d). As a matter of fact, various intermediate steps involved in the overall pyruvate preparative reduction occur in sort of steady state, as revealed by the fairly flat profiles of the current, fraction θ and NAD^+ significance (Figure 9b, c, d). Simulation conducted until complete conversion showed that the three above variables suddenly decayed from conversion over 95%. Then oxidant species Rh(III) and NAD^+ rapidly decayed for nearly complete conversion conditions. Although with nuances depending on operating conditions,

the system appears to operate at steady state with respect of most variables, except for pyruvate concentration for the main part of the conversion.

Another fact to be mentioned from Figure 9 linked to parameters values given above, is that θ is low, i.e. noticeably below 0.5 – Rh complex is mainly monovalent, indicating that the electrochemical reduction of immobilized Rh(III) is no rate-controlling process. Moreover, the very large NAD^+ significance – over 0.97 in Figure 9, would express that NAD^+ reduction by electrogenerated Rh(I) complex is rate-controlling.

Effects of the model kinetic parameters

The effect of these parameters has observed on the preparative reduction to better understand the possible rate control of one of them, depending on the conditions used. The variables of interest to characterize the progress of reduction were (i) lactate concentration, (ii) cell current, (iii) surface fraction θ, and (iv) NADH bulk concentration, all of them after 6 hours reduction in the presence of 10 µM NADx in 100 mL PBS solution. For this purpose, one parameter was varied while the two others were kept at their "reference" levels given above.

- Max. enzymatic reaction rate v_{max} below 1.2 10^{-5} mol m^{-2} s^{-1} (0.02 µmol mg^{-1} s^{-1}) appears to be rate controlling as shown by the nearly linear increase in lactate concentration, cell current and surface fraction θ (Figure 10a). In the meanwhile, NADH bulk concentration decreased regularly from 10 to 2 µM (Figure 10b). Beyond this rate, the beneficial effect of v_{max} is less visible and become poorly significant beyond 2 10^{-5} mol m^{-2} s^{-1}, the conversion being then controlled by the two other parameters.
- Control from chemical reaction constant rate k_c is also visible for k_c below 15-20 m^3 mol^{-1} s^{-1} as shown in Figure 10c and d, with the regular increase in pyruvate reduction rate, cell current, fraction θ and NADH concentration. It can be observed that NADH in the bulk represents only 10% of the overall NADx concentration and θ is only at 0.15 for k_c = 18 m^3 mol^{-1} s^{-1}: NAD^+ and Rh(III) are the prevailing forms of the two mediators for this k_c value. Increasing further k_c improves the reduction progress, however to a restricted extent, because of the limits imposed by v_{max} and k_e.
- Increase in electrochemical reaction rate k_e is also obviously beneficial for the conversion (Figure 10e and f), however in a restricted domain: beyond 0.3 s^{-1}, the effect of k_e on lactate formation, fraction θ, current I and NADH concentration become far less significant. For

this k_e value, θ is near 0.2 and NADH represents only 2% of the NADx introduced: again, the mediators of the bioelectrochemical reduction are mainly on the form of NAD^+ and Rh(I). For k_e greater than 0.6 s^{-1}, the various variables vary very little and in particular, NADH concentration cannot attain 0.4 µM (Figure 10f), i.e. 4% of the NADx concentration.

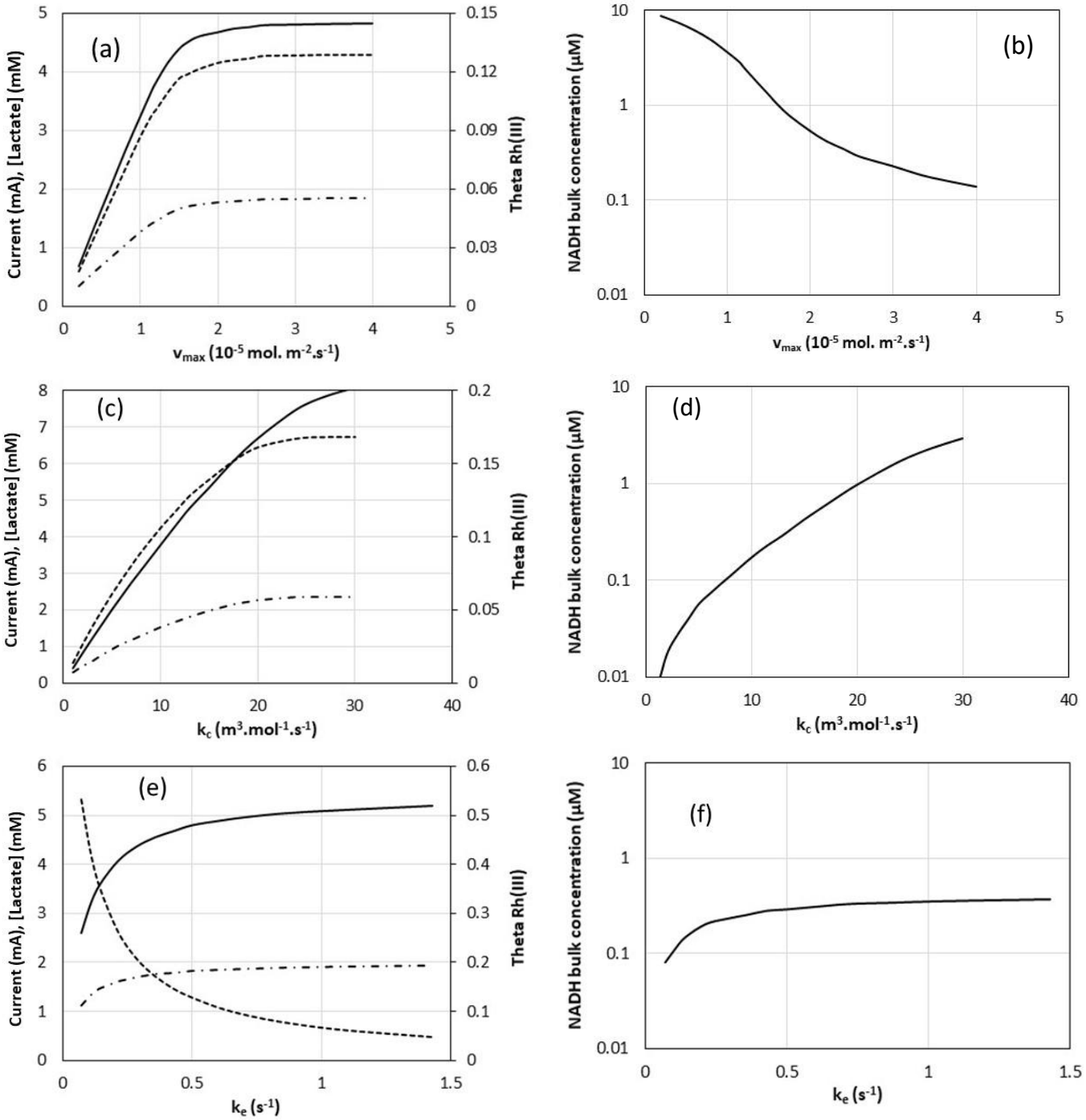

Figure 10: Simulation of LDH-catalyzed reduction of pyruvate with Rh complex and NAD^+/NADH mediation in the flow reactor. NADx concentration at 10 µM, Solution

volume=100 mL, area S = 16 cm^2 and E cathode = -0.4 V vs. Ref. H_2. Effect of v_{max} (Figs. 10a and b), k_c (Figs. 10c and d) and k_e (Fig.s 10e and f) on several variables after 6 hours electrolysis: (_____): bulk concentration of lactate formed, (_._._): cell current, (------): fraction θ for Rh(III) and NADH bulk concentration

It appears from Figures 9 and 10 that the overall rate of pyruvate reduction is mainly controlled by the enzymatic process and to a larger extent by the kinetics of the redox reaction at the electrode surface between Rh(I) complex and NAD^+. Whereas enhancement of the enzymatic reaction rate can be easily obtained by immobilizing more enzymes or by further improvement of its wiring, the rate of Rh(III) reduction and of NADH regeneration are strongly related to each other in the present configuration of immobilized Rh complexes. The cell configuration renders the rates highly depending since grafting more Rh complex onto the CP-MWCNT support would also result in higher electrochemical reduction rate, still under comparable control of the surface redox reaction between NAD+ and Rh(I) complex.

5- Conclusions

A model of the overall bioelectrochemical process for LDH-catalyzed reduction of pyruvate has been developed by direct superimposition of the various processes to explain the high lactate production (up to 0.8 10^{-5} mol m^{-2} s^{-1}) with high TTN for NADx concentrations as low as 10 µM. In this concentration domain, mass transfer coefficients larger than 10^{-3} ms^{-1} had to be considered, as justified by considering the expression of the various mass transfer rates in the model equations. This suggested occurrence of process intensification. Moreover, higher redox reaction rates between NAD^+ and electrogenerated Rh(I) complex had to be used in simulations: the hypothesis was confirmed by NADH regeneration tests conducted with 100 µM NAD^+ introduced. More extensive investigation of the redox reaction with immobilized Rh complex would nevertheless be required.

This work also revealed that the physics of coupled transfer and reaction processes in small-scale systems has still to be better understood, for a more precise comprehension of the word intensification, often employed when observing high production rates and TTN, but without quantitative explanations. Moreover, this would allow more precise analysis of these processes and their better-controlled occurrence in the design of a new production process. Nevertheless, the model and the analytical approach for identification of rate-controlling step(s), could be applied to other cell configurations or to other reaction examples such as CO_2 reduction with formate dehydrogenase.

Conflict of interest:

The authors declare that there is no conflict in interest

Acknowledgements: Thanks are due to CNRS for the inter-department PhD grant allocated to W. El Housseini and to contribution to the research costs.

Author's contributions

W. El Housseini: Investigation; Methodology; M. Etienne: Funding acquisition; Supervision; Writing - review & editing; E. Lojou: Funding acquisition; Investigation; Supervision; Editing; A. Walcarius: Review & editing; F. Lapicque: Funding acquisition; Project Modelling; Writing - review & editing.

References cited

[1] E. Steckhan, E., Electroenzymatic Synthesis, Top. Curr. Chem. 170, 83-111, Springer-Verlag, Berlin Heidelberg (1994).

[2] Kohlmann, C., Märkle, W., Lütz, S.. Electroenzymatic Synthesis, J. Mol. Catal. B 51(3-4) (2008) 57-72. doi:10.1016/j.molcatb.2007.10.001.

[3] H.K. Chenault, G.M.Whitesides, Regeneration of Nicotinamide Cofactors for use in Organic Synthesis. Appl. Biochem. Biotechnol. 14(2) (2007) 147-197. doi:10.1007/BF02798431.

[4] S. Immanuel, S., Sivasybramanian, R, Gul, R., Dar, MA., Recent progress and perspectives on electrochemical regeneration of reduced nicotinamine adenine dinucleotide, Chem. Asian J. 15(24) (2020) 4256-4270. doi: 10.1002/asia.202001035.

[5] H. Jaegfeldt, A study of the products formed in the electrochemical reduction of nicotinamide-adenine-dinucleotide, J. Electroanal. Chem. 128 (1981) 355-370. doi:10.1016/S0022-0728(81)80230-6.

[6] H.C. Lo, O. Buriez, J.B. Kerr, R.H. Fish, Regioselective reduction of NAD+ models with $[Cp^*Rh(bpy)H]^+$ structure: structure-activity relationships and mechnistric aspects in the formation of the 1,4-NADH derivative, Angew. Chem. Int. Ed. 38(10) (1999) 1429-1432. doi: 10.1002/(SICI)1521-3773(19990517)38:10<1429: AID-ANIE 1429>3.0.CO;2-Q.

[7] F. Hollmann, B. Wilholt, A. Schmid, $[Cp^*Rh(bpy)(H_2O)]^{2+}$: a versatile tool for efficient and non-enzymatic regeneration of nicotinamide and Flavin coenzymes, J. Mol. Catal. B 19-20 (2003) 167-176. doi: 10.1016/S1381-1177(02)00164-9.

[8] E. Höfer, E., Steckhan, E., Ramos, B., Heineman, W.R., Polymer-modified electrodes with pendant $[Rh^{III}(C_5Me_5)(L)Cl]^+$-complexes formed by γ-irradiation cross-linking, J. Electroanal. Chem. 402(1-2) (1996) 115-122. doi:10.1016/0022-0728(95)04243-1.

[9] L.M.A. Quintana, S.I. Johnson, S.L. Corona, W. Villatoro, W.A. Goddard III, M.K. Takase, D.G. VanderVelde, H.R. Gray, J. Blakemore. Proton-hybride tautomerism in hydrogen evolution catalysis. PNAS, 113(23) (2016) 6409-6414. doi :10.1073/pnas.1606018113.

[10] E.A. Boyd, D. Lionetti, W.C. Henke, V.W. Day, J.M. Blakemore, 2018. Preparation, characterization, and electrochemical characterization of a model [Cp*Rh] hydride. Inorg. Chem. 58 (2019) 3606-3615. doi: 10.1021/acs.inorgchem.8b02160.

[11] S. Pal, S. Kusumoto, K. Nozaki. Dehydrogenation of dimethylamine-borane catalysed by half-sandwich Ir and Rh complexes: Mechanism and the role of CP* noninnonence, Organometallics 37 (2018) 906-914. doi:10.1021/acs.organomet.7b00889.

[12] W. El Housseini, M. Etienne, A. Walcarius, F. Lapicque. Multiphase engineering as a tool in modelling electromediated reactions – example of Rh complex-mediated regeneration of NADH, Chem. Eng. Sci. 247 (2022) 117055. doi: 10.1016/j.ces.2021.117055.

[13] P.V. Danckwerts, Gas-liquid reactions, McGraw-Hill, New-York (1970).

[14] W. El Housseini, F. Lapicque, A. Walcarius, M. Etienne, A hybrid electrochemical flow reactor to couple H_2 oxidation to NADH regeneration for biochemical reactions, Electrochem. Sci. Adv. (2021) e2100012. doi: 10.1002/elsa.202100012.

[15] W. El Housseini, F. Lapicque, S. Pontvianne, N. Vila, I. Mazurenko, A. Walcarius, M. Etienne, Hybrid flow bioreactor with all catalysts immobilized for enzymatic electrosynthesis, ChemElectroChem (2022) 9 e202200463. doi: 10.1002/celc.202200463.

[16] B. Limoges, D. Marchal, F. Mavré, J.M. Savéant, Electrochemistry of immobilized redox enzymes: kinetic characteristics of NADH oxidation catalysis at diaphorase monolayers affinity immobilized on electrodes, J. Am. Chem. Soc. 128 (2006) 2084-2092. doi: 10.1021/ja0569196.

[17] F. Alam, S. Roy Choudhuryn, A.H. Jala, Y. Umasankar, S. Forousankar, N. Akter, S. Bhansali, N. Pala, Lactate biosensing: the merging point-of car and personal health monitoring, Biosens. Biolectron. 117 (2018) 218-829. doi:10.1016/j.bios.2018.06.054.

[18] Z. Nate, A.A.S. Gill, R. Chauhan, R. Karpoormath, Recent progress in electrochemical sensors for detection and quantification of malaria, Anal. Biochem. 643 (2022) 114592. doi: 10.1016/j.ab.2022.114592.

[19] H. Deng, N. Zhadin, R. Callender, Dynamics of protein ligand binding on multiple time scales: NADH binding to lactate dehydrogenase, Biochemistry 40 (2001) 767-3773. doi:10.1021/bi0026268.

[20] D.K. Shoemark, M.J. Cliff, R.B. Sessions, A.R. Clarke. Enzymatic properties of the lactate dehydrogenase enzyme from Plasmodium Falciparum, FEBS J. 274 (2007) 2738-2748. doi: 10.1111/j.1742-4658.2007.05808.x.

[21] J.R. Exequiel, T. Pinade, R. Callender, S.D. Schwartz, Ligand binding and protein dynamics in lactate dehydrogenase, Biophys. J. 93 (2007) 1474-1483. doi: 10.1529/biophysj.107.106146.

[22] J.M. Hernandez-Meza, J.G. Sampedro, Trehalose mediated inhibition of lactate dehydrogenase from rabbit muscle. The application of Kramer's theory in enzyme catalysis, J. Phys. Chem. B 122 (2018) 4309-4317. doi: 10.1021/acs.jpcb.8b01656.

[23] W. Ehrfeld, U. Ehrfeld, Microfabrication for process intensification, In: Matlosz, M., Ehrfeld, W., Baselt, J.P. (eds) Microreaction Technology. Springer, Berlin, Heidelberg (2001). doi: 10.1007/978-3-642-56763-6_1.

[24] F.W. Scheller, C.G. Bauer, A. Makower, U. Wollenberger, A. Warsinke, F.F. Bier. Coupling of immunoassays to enzymatic recycling electrodes, Anal. Lett. 34 (2001) 1233-1245. doi: 10.1081/AL-100104149.

[25] B. Limoges, D. Marchal, F. Mavré, J.M. Savéant, High amplification rates from the association of two enzymes confined within a nanometric layer immobilized on an electrode: Modelling and illustration example, J. Am. Chem. Soc. 128 (2022) 6014-6015. doi: 10.1021/ja060801n.

[26] B. Poznansky, S.E. Cleary, L.A. Thompson, H.A. Reeve, K.A. Vincent, Boosting the productivity of H_2-driven biocatalysis in a Commercial Hydrogenation Flow reactor using H_2 from water electrolysis. Front. Chem. Eng., 35(3) (2021) 718257. doi: 10.3389/fceng.2021.718257.

[27] L. Zhang, M. Etienne, N. Vila, T.X. Huong Lee, G-W. Kohring, A. Walcarius. Electrocatalytic biosynthesis using a bucky paper functionalized by $[Cp^*Rh(bpy)Cl]^+$ and a renewable enzymatic layer, ChemCatChem 10 (2018) 4067-4073. doi: 10.1002/cctc.201800681.

[28] A. Walcarius, R. Nasraoui, Z.Wang, F. Qu, V. Urbanova, M. Etienne, M. Göllü, J. Gajdzik, M. Hempelmann. Factors affecting the electrochemical regeneration of NADH by (2,2′-bipyridyl) (pentamethylcyclopentadienyl)-rhodium complexes: Impact on their immobilization onto electrode surfaces, Bioelectrochemistry 82 (1) (2011) 46-54. doi:10.1016/j.bioelechem.2011.05.002

[29] M.J. Doughty, Some kinetic properties of lactate dehydrogenase activity in cell extracts from a mammalian (ovine) corneal Epithelium, Exp. Eye Res. 66 (1998) 231-239. doi: 10.1006/exer.1997.0423.

[30] H.C. Lo, C. Leiva; O. Burliez, J.B. Kerr, M.M. Olmstead, R.H. Fish, Bioorganometallic chemistry. 13. Regioeslective reduction of NAD^+ models, 1-benzylnicotinamide triflate and b-nicotonamide ribose-5'-methyl phosphate, with in situ generated $[Cp^*Rh(bpy)H]^+$: structure-activity relationships, kinetics and mechanistic aspects in the formation of the 1,4- NADH derivatives, Inorg. Chem. 40 (2001) 6703-6016. doi: 10.1021/ic010562z.